THE JOURNAL OF PHYSICAL CHEMISTRY C

Article

Cite This: J. Phys. Chem. C 2019, 123, 19786−19793

pubs.acs.org/JPCC

Variations in Atomic-Scale Step Edge Structures and Dynamics of Dissolving Calcite in Water Revealed by High-Speed Frequency Modulation Atomic Force Microscopy

Kazuki Miyata,[†,‡] Yuta Kawagoe,[‡] John Tracey,[§] Keisuke Miyazawa,[†,‡] Adam S. Foster,[*,§,†] and Takeshi Fukuma[*,†,‡]

[†]Nano Life Science Institute (WPI-NanoLSI) and [‡]Division of Electrical Engineering and Computer Science, Kanazawa University, Kakuma-machi, Kanazawa 920-1192, Japan

[§]Department of Applied Physics, Aalto University, Helsinki FI-00076, Finland

Supporting Information

ABSTRACT: Calcite dissolution plays critical roles in the global carbon cycle in the Earth, biomineralizations, and weathering of buildings. However, in spite of the importance, the atomistic events at the step edges during the dissolution have remained elusive because of the difficulties in their direct visualization. In this study, we used high-speed frequency modulation atomic force microscopy (FM-AFM) for visualizing various atomic-scale step edge structures and dynamics during the calcite dissolution in water. The obtained images reveal the coexistence of the steps with and without a transition region (TR); a $Ca(OH)_2$ monolayer formed along the step edge as an intermediate state in the dissolution. The TRs are more frequently observed along the slowly dissolving acute steps than along the rapidly dissolving obtuse steps. This finding and our imaging of the TR formation process suggest that the free energy to form a TR is comparable to that for removing ions directly from the step edge and an increase in the local ionic strength may alter this balance to facilitate the TR formation. Once the TRs are formed, their width or height shows no significant dependence on the crystallographic orientation or the step velocity. We also found that the FM-AFM images of the TRs show several variations. However, the hydration structures obtained by our molecular dynamics simulation demonstrate that the observed variations can be explained by the different tip trajectories on the different hydration layers. These findings should improve our understanding on both the calcite dissolution mechanism and the FM-AFM measurement principle.

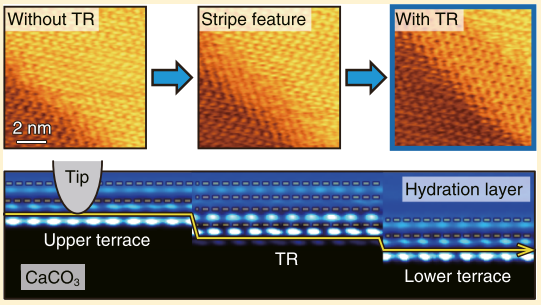

INTRODUCTION

Calcite ($CaCO_3$) is the largest carbon reservoir in the Earth, and its reaction plays important roles in the global carbon cycle.[1−3] For example, the calcite dissolution affects global landforms, climate, and the aqueous environment through the changes in the CO_2 concentration in the atmosphere and pH of the environmental water.[4] In addition, the calcite dissolution is also closely related to the biomineralization,[5,6] weathering of buildings and monuments,[7] and CO_2 leakage in the geological carbon sequestration.[8] For understanding, predicting, and controlling these phenomena and processes, the mechanisms of calcite dissolution have widely been investigated. These previous studies include macroscopic elemental flow analyses using a flow-through reactor, microscopic step flow analyses by atomic force microscopy (AFM) or optical interferometry,[9−14] and theoretical simulations by molecular dynamics (MD), kinetic Monte Carlo (MC), or density functional theory.[14−19] These previous works enabled us to describe the macroscopic dissolution behavior by an analytic rate equation with semiempirically determined parameters and reproduce some of the nanoscale dynamics of the dissolving calcite surfaces by kinetic MC simulation.

However, the atomic-scale physical and chemical processes at the step edges during the dissolution are yet to be understood. Such atomistic events are the most fundamental steps in the whole dissolution process and hence their understanding is essential for its robust simulation, prediction, or control under various environments. One of the major problems in such studies is the lack of an in situ imaging technique. While AFM is one of the most promising candidates to solve this problem, conventional AFM techniques do not have either sufficient spatial or temporal resolution. For example, Ando et al. developed high-speed amplitude-modulation AFM with a speed of 10−100 ms/frame and enabled to image nanoscale dynamics of proteins in liquid.[20] However, spatial resolution of conventional high-speed AFM is limited to ∼1 nm. In the meantime, Fukuma et al. enabled to

Received: June 18, 2019
Revised: July 24, 2019
Published: July 24, 2019

DOI: 10.1021/acs.jpcc.9b05788
J. Phys. Chem. C 2019, 123, 19786−19793

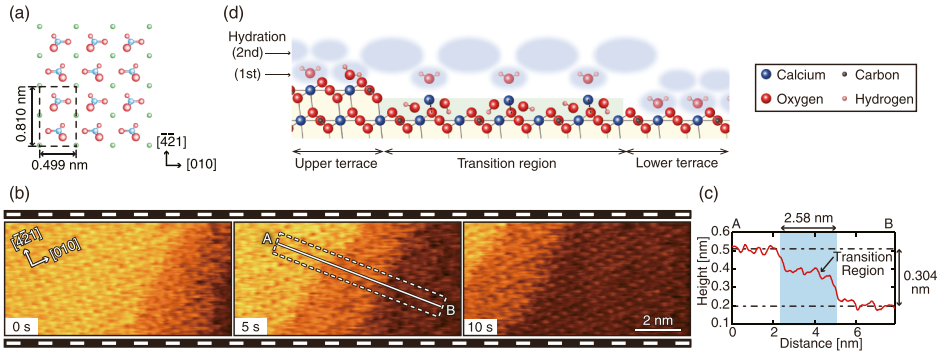

Figure 1. High-speed FM-AFM images of calcite dissolving in water and the atomistic model of the step edge. (a) Atomistic model of the calcite ($10\bar{1}4$) surface. (b) Snapshots of the successive FM-AFM images of the calcite surface in water. Imaging speed: 0.5 s/frame. Scan size: 10 × 5 nm^2. Pixel size: 500 × 250 pix^2. (c) Average height profile measured along line A–B indicated in (b). The dotted lines around line A–B indicate the width of the averaging. (d) Atomistic model of the step edge with a TR made of $Ca(OH)_2$.

operate frequency modulation AFM (FM-AFM) with atomic resolution in liquid and visualized subnanometer-scale surface structures and hydration structures at solid–liquid interfaces.[21,22] However, the speed of the conventional FM-AFM was limited to ∼1 min/frame, which is often insufficient to visualize dynamics related to crystal growth or dissolution.

To achieve sufficient spatial and temporal resolution, we have recently developed high-speed FM-AFM that allows us to perform atomic resolution imaging in liquid at ∼1 s/frame.[23−31] With the developed system, we directly imaged atomic-scale structural changes at the step edges during calcite dissolution in water.[32] The obtained images revealed the formation of a characteristic transition region (TR) along the step edges with an intermediate height between the upper and lower terraces and a width of a few nanometers. In addition, we performed simulations with various possible models of the step edge structures and found that the observed TR is most likely to be a $Ca(OH)_2$ monolayer formed as an intermediate state in the dissolution process. Based on this finding, we proposed an atomistic calcite dissolution model to explain the atomistic events happening at the step edges during the dissolution.

The finding of the TR should give significant impacts on the current discussions on the dissolution mechanisms. For example, it has been well known that the dissolution kinetics are greatly influenced by an adsorption of ions or molecules at the step edges and such an adsorption is sensitive to the atomistic features such as kinks and hydration layers.[33,34] Therefore, the formation of the TR should be taken into account when we perform a simulation or interpretation of experimental results. However, little is known on the properties of the TR, and hence, it is difficult to quantitatively associate it with a specific issue on the dissolution mechanism. For example, it has not been clarified if the step edge always shows a TR with the same height and width. If there are any variations, their dependence on the crystallographic orientations and step velocity should be statistically analyzed. In addition, we should also address if the observed images reflect the real surface topography. This is because AFM images of the same structure can show different image contrasts because of the variations in the tip apex conditions or other experimental parameters.[35] In particular, such apparent variations become evident at solid–liquid interfaces, as the tip can be scanned either on the solid surface or on one of the hydration layers.[36]

In order to answer these fundamental questions, we have performed a systematic study on the atomic-scale step edge structures of calcite observed by high-speed FM-AFM during the dissolution in water. We present several variations in the observed step edge structures and discuss possible origins of the variations based on the simulated hydration structures and different tip scan trajectories on them. In addition, the obtained images are statistically analyzed to understand the relationship between the observed variations and the crystallographic orientation, the step velocity, and the width and height of the TRs.

EXPERIMENTAL SECTION

AFM Experiment. In this study, we used a calcite substrate (Crystal Base Co, Ltd.) with a size of 5 × 5 × 2 mm^3. The substrate was glued to the sample holder. Immediately after the cleavage of the substrate, 50 μL of Milli-Q water was added dropwise to the sample surface. In the dropwise added water, we performed high-speed FM-AFM imaging in the constant frequency shift mode at room temperature. For all experiments, we used the commercially available silicon cantilevers (AC55, Olympus), with a typical spring constant k, quality factor Q, and resonance frequency f_0 in an aqueous environment of 80 N/m, 10, and 1.5 MHz, respectively. To eliminate the contaminants on the tip surface, the tip was coated with a 15 nm silicon film by a dc sputter coater (K575XD, Emitech).[37] For high-speed FM-AFM operation with atomic-scale resolution, we used the custom-built FM-AFM setup with the low-noise cantilever deflection sensor,[23−25] highly stable photothermal cantilever excitation system,[25,26] high-speed scanner,[27,28] low-latency wideband phase-locked loop, and FM-AFM controller.[29−31]

MD Simulation. The detailed methods for the MD simulation were previously reported elsewhere.[38,39] Thus, here we only describe them briefly. All simulations were performed using the MD code large-scale atomic/molecular massively parallel simulator,[40] and analysis was performed visually using visual molecular dynamics or numerically by bespoke code using the Python library MD analysis.[41,42] For this system, the same force field is used for the MD simulations as in the previous work.[32] In that work, we tested different setups with several species for investigating the origins of the TR and found calcium hydroxide as the most likely model.

RESULTS AND DISCUSSION

Typical Step Edge Structure. In the previous study, we reported the typical high-speed FM-AFM images of the

DOI: 10.1021/acs.jpcc.9b05788
J. Phys. Chem. C 2019, 123, 19786−19793

dissolving calcite step in water and their interpretation. Here, we show another example of such typical images and thereby briefly explain the reported interpretation and model to explain the dissolution mechanism (Figure 1). The cleaved calcite surface consists of calcium and carbonate ions as shown Figure 1a. Figure 1b shows three snapshots selected from the successive FM-AFM images (see Movie S1 consisting of all of the successive images). In these images, the atomic step retreating from the right to the left is visualized. Figure 1c shows the average height profile measured along line A−B in Figure 1b. This profile reveals that the height difference between the upper and lower terraces is ∼0.3 nm, which corresponds to the height of a single atomic step on the calcite $(10\bar{1}4)$ surface (0.304 nm). In addition, this profile also shows the existence of a TR having a height of ∼0.2 nm from the lower terrace. Our previous study showed that this TR is most likely to be a $Ca(OH)_2$ monolayer formed as an intermediate state in the calcite dissolution (Figure 1d).[32]

The imaging mechanism of this TR is explained by the simulated water density map as shown in Figure 2. This figure shows the formation of at least three hydration layers on the upper and lower terraces (U1−U3 and L1−L3) and five layers on the TR (T1−T5) as indicated by the arrows in Figure 2. As demonstrated in the previous study, the tip can be scanned on one of these hydration layers.[32] Thus, there exist many possible tip trajectories. By comparing these trajectories with an experimentally measured height profile across the step edge (e.g., Figure 1c), we can narrow down the possible tip trajectories. For example, in the previous study, we determined the tip trajectory U1 → T1 → L1 indicated by the yellow dotted line in Figure 2 for the typical appearance of the TR with an intermediate height between the upper and lower terraces (e.g., Figure 1b).

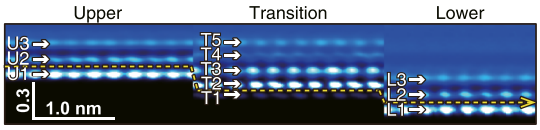

Figure 2. MD simulation of the calcite $(10\bar{1}4)$ surface in water with the TR made of $Ca(OH)_2$. The $[\bar{4}41]$ projection of the water density map obtained by averaging the simulated distribution over each unit cell area. The white arrows show the hydration layers, whereas the yellow dotted line shows the expected tip trajectory for the image shown in Figure 1b.

In the following discussions, we present the FM-AFM images showing different step edge structures and their dynamic changes. We demonstrate that these variations can be largely explained by the combinations of the different tip trajectories (U1−3, T1−5, L1−3) indicated in Figure 2. We do not individually discuss possible influence of the scan artifacts caused by the feedback errors, set point drifts, or nonideal tip geometry to avoid repeated discussions on the same point. Instead, we discussed these points in the Supporting Information with additional FM-AFM images (Figures S1−S5).

Variations in the Step Edge Structure. Figure 3a shows the successive FM-AFM images of the dissolving calcite steps showing a contrast change during the imaging (see Movie S2 consisting of all of the successive images). At 0 and 5 s, the TRs with an intermediate height (∼0.16 nm) between the upper and lower terraces are observed along the step edges as confirmed by the height profile A−B (Figure 3b). However, the appearance of these TRs was changed at 10 s and then remained to be imaged as a depression. The apparent depth of this depression is 0.071 nm from the lower terrace as confirmed by the height profile C−D (Figure 3c). By comparing the height profiles shown in Figure 3b,c with the hydration structure at the step edge, this contrast change can be explained by the change of the tip trajectory from U3 → T4 → L3 (before 5 s) to U3 → T2 → L3 (after 10 s).

Such a dynamic change in the tip trajectory can be caused by the changes in the local ion concentration or tip apex structure. While this experiment was performed in pure water, calcite dissolution should produce interfacial ions diffusing near the surface, which may induce time-dependent variations in the local ionic strength. The force versus distance curve measured by FM-AFM in liquid is known to be sensitive to the local solution condition and tip apex structure. Therefore, it is reasonable to expect that such a slight change in the force versus distance curve should cause a discontinuous change in the tip trajectory.

Figure 3e shows another example of the FM-AFM images showing a contrast change during the imaging (see Movie S3 consisting of all of the successive images). At 0 s, a depression is observed along the step edge. The height profile E−F (Figure 3f) shows that the apparent depth from the lower terrace is 0.22 nm, which is slightly deeper than the one observed in Figure 3c. In addition to this depression, we also found another characteristic region with a few nanometer width at the edge of the upper terrace (the gray background region in Figure 3f,g). At 0 s, the height of this region is almost the same as that of the upper terrace. However, it was lowered by 0.26 nm at 10 s (Figure 3f). Thus, two TRs with different heights exist at 10 s.

Figure 3h shows the tip trajectories expected from the height profiles. The height difference between the depressed area and lower terrace suggests that the tip was scanned on T1 at the depressed region and on U3 and L3 at the upper and lower terraces, respectively. At the edge of the upper terrace, the tip was scanned on T5 at 0 s because this layer has almost the same height as U3. At 10 s, the tip position on the TR was changed from T5 to T3. Note that fine stripes observed on the upper terrace almost seamlessly extend over this region as indicated by the arrows. This result indicates that the hydrogen bonding network formed on the upper terrace is extended over the TR. This is consistent with the simulated hydration structure and the previously reported explanation for the energetic merit to form the TR at the step edges.[32]

Similar to the discussion that we made for Figure 3a, the dynamic change of the tip trajectory can be explained by the changes in the local ionic strength or the tip apex structure. As for the discontinuous jump of the tip position in the middle of the TR, a few possible reasons can be suggested. First, the $Ca(OH)_2$ layer formed along the step edge should not be perfectly uniform but it should vary as a function of the distance from the upper terrace edge. Similarly, the local distribution of the interfacial ions should not be uniform due to the difference in the chemical reactions at the upper and lower terrace edges. Such a gradation in the surface structure and local ionic strength should result in a gradual change in the force versus distance curve. As the tip position can only take one of the discrete positions, the gradual change of the force profile will lead to the discontinuous change in the tip trajectory in the middle of the TR.

DOI: 10.1021/acs.jpcc.9b05788
J. Phys. Chem. C 2019, 123, 19786−19793

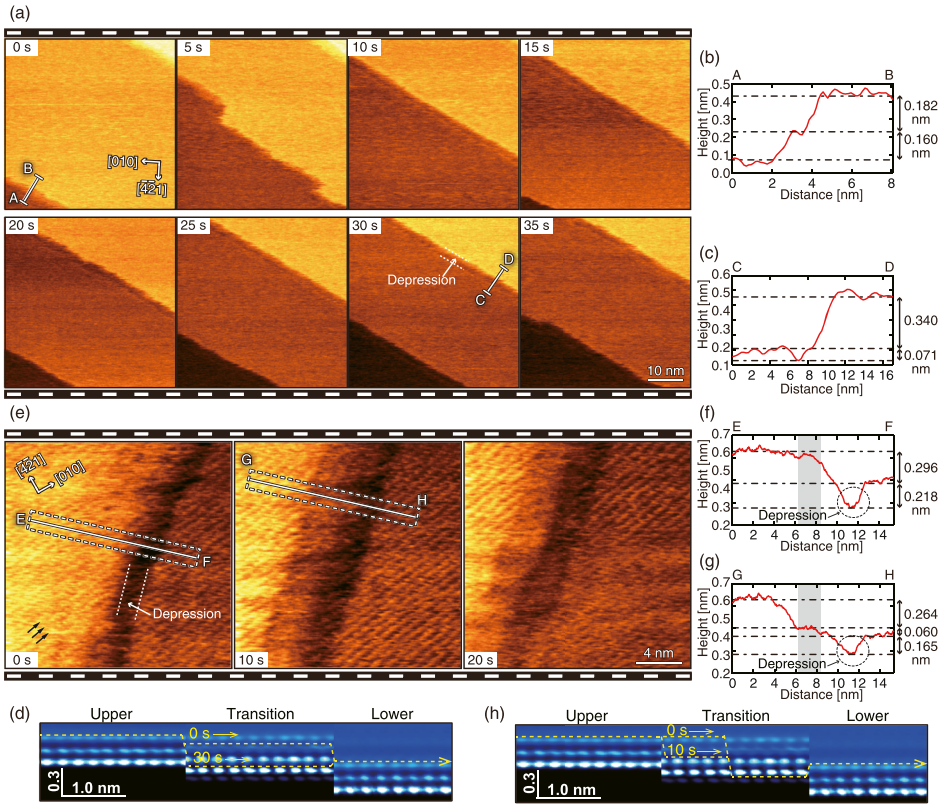

Figure 3. High-speed FM-AFM images of calcite dissolving in water with various TR appearances. (a) Successive FM-AFM images of the calcite surface in water. Imaging speed: 5 s/frame, scan size: 50 × 50 nm^2, pixel size: 500 × 500 pix^2. (b,c) Average height profiles measured along line A−B and C−D indicated in (a). (d) Tip trajectories that can account for the height profiles in (b,c). (e) Successive FM-AFM images of the calcite surface in water. Imaging speed: 10 s/frame, scan size: 20 × 20 nm^2, pixel size: 500 × 500 pix^2. (f,g) Average height profiles measured along lines E−F and G−H indicated in (e). (h) Tip trajectories that can account for the height profiles in (f,g).

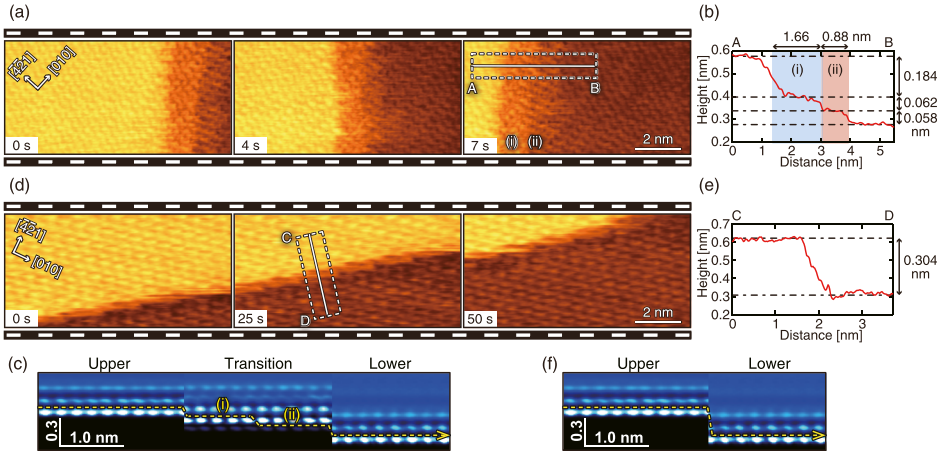

Figure 4. High-speed FM-AFM images of calcite dissolving in water with various appearances of the step edges. (a) Snapshots of the successive FM-AFM images showing the step edge with the two-divided TR. Imaging speed: 1 s/frame, scan size: 10 × 5 nm^2, pixel size: 500 × 250 pix^2. (b) Average height profile measured along line A−B indicated in (a). (c) Tip trajectory that can account for the height profile in (b). (d) Snapshots of the successive FM-AFM images without a TR. Imaging speed: 0.5 s/frame, scan size: 10 × 5 nm^2, pixel size: 500 × 250 pix^2. (e) Average height profile measured along line C−D indicated in (d). (f) Tip trajectory that can account for the height profile (e).

Figure 4a shows the snapshots of the successive FM-AFM images showing another two-divided TR (see Movie S4 consisting of all of the successive images). In the images, four areas with different heights are visualized. The height difference between the highest and lowest areas is 0.304 nm, which approximately equals to the height of the single molecular step (Figure 4b). Thus, the intermediate two regions should correspond to the two-divided TR. Unlike the structure observed in Figure 3e, the lower half of the TR is still higher than the lower terrace. Comparison between the height profiles and hydration structure reveals that there are three possible tip trajectories U1 → T2 → T1 → L1, U2 → T3 → T2 → L2, and U3 → T4 → T3 → L3. Although we cannot conclusively determine a single trajectory, we suggest the

DOI: 10.1021/acs.jpcc.9b05788
J. Phys. Chem. C 2019, 123, 19786−19793

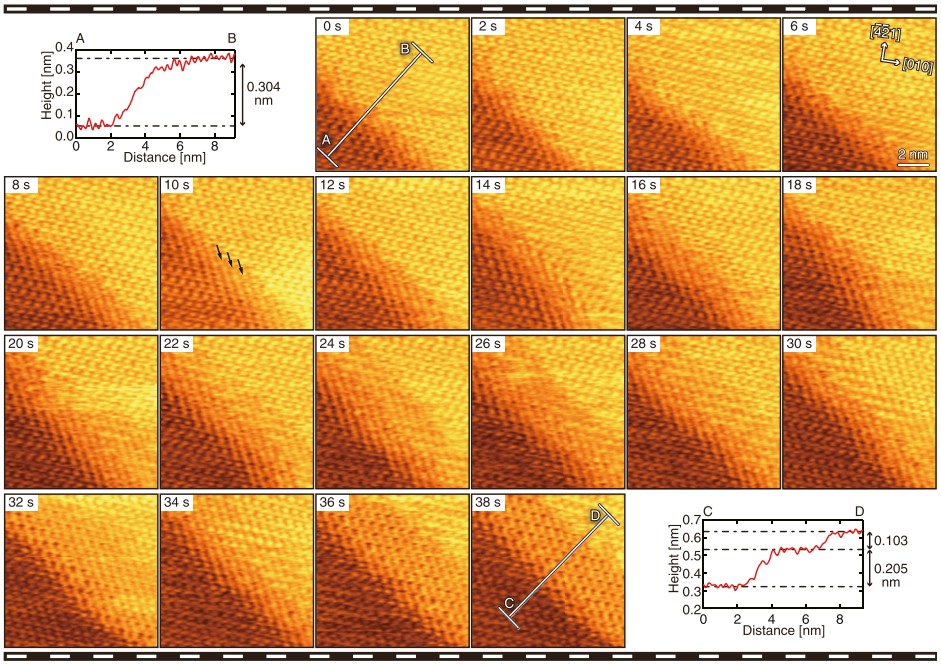

Figure 5. Snapshots of the successive FM-AFM images of the dissolving calcite in water and average height profiles measured along lines A−B and C−D indicated in the images obtained at 0 and 38 s. Imaging speed: 2 s/frame, scan size: 10 × 10 nm^2, pixel size: 500 × 500 pix^2.

trajectory U1 → T2 → T1 → L1 as the most plausible model because of the clear atomic-scale contrasts observed on the upper and lower terraces. This two-divided TR can be explained by the same imaging mechanism that we suggested for the images shown in Figure 3e.

Figure 4d shows the snapshots of the successive FM-AFM images of the dissolving calcite step without a TR (see Movie S5 consisting of all of the successive images). The height profile measured across the step shows no plateau corresponding to a TR (Figure 4e). These results suggest that $CaCO_3$ molecules at the step edge desorb from the surface without forming an extended layer of $Ca(OH)_2$. Strictly speaking, we can see a narrow intermediate region with an atomic-scale width (<0.5 nm). Thus, there may be a single $Ca(OH)_2$ row adsorbed at the step edge. However, this width roughly corresponds to the expected width of the irregular hydration structure formed along the step edge even without any adsorption of $Ca(OH)_2$ molecules.[15,32] Therefore, here, we define such steps with an intermediate region having a width less than 0.5 nm as a "step without a TR". The imaging mechanism of such steps can be explained by the tip trajectory U1 → L1, U2 → L2, or U3 → L3. Although we cannot uniquely determine the tip trajectory, the clear atomic-scale contrasts observed in the images suggest that the tip trajectory U1 → L1 (Figure 4f) may be most plausible.

Formation Process of the TR. Among the 117 steps observed in our experiments, 27 steps were imaged without an extended TR, which correspond to ∼23% of the whole steps. Thus, they are less common and may be energetically unfavorable compared to the steps with a TR. In fact, we were able to observe the formation of a TR during the imaging as shown in Figure 5 (see Movie S6 consisting of all of the successive images). From 0 to 6 s, there is no extended TR as confirmed by the height profile A−B. From 8 to 26 s, an intermediate region showing stripe features indicated by arrows in Figure 5 is gradually formed and grows in the width. From 28 to 34 s, the stripe features become less evident. At 36 s, a clear TR with a width of 3−4 nm is formed as confirmed by the height profile C−D.

During the imaging, the step position showed almost no change. The estimated step velocity (0.06 nm/s) is much slower than the average value measured in our experiment for this crystallographic orientation (0.431 nm/s). This result suggests that the adsorption and desorption of the ions during the imaging were nearly balanced. Thus, the dissolved ions were probably diffusing around the step edge. This idea is also consistent with the other observations. For example, the stripe features were once formed at 26 s but soon disappeared at 32 s, which indicates that the local solution condition is close to the equilibrium value. In addition, the edge of the stripe features shows blurred contrasts, suggesting the rapid adsorption and desorption of the ions at the step edge compared to the imaging speed.

According to the previous study, the chemical reactions during the calcite dissolution at the step edge can be described by the following formulae.[32]

$$CaCO_3 + H_2O \rightarrow CaOH^+ + HCO_3^- \quad (1)$$

$$CaOH^+ + HCO_3^- \rightarrow Ca(OH)_2 + CO_2 \quad (2)$$

Therefore, the observed TRs can be explained by the two possible models: a $CaOH^+$ monolayer with diffusing HCO_3^- ions or a $Ca(OH)_2$ monolayer. In our previous study, our MD simulation suggested that the latter model is much more stable and consistent with the clear atomic-scale contrasts observed by FM-AFM.[32] Thus, we attributed the observed TR to the $Ca(OH)_2$ monolayer. In this study, we observed the striped features showing a large fluctuation as an intermediate state to form the stable TR. This may be explained by the transient formation of a $CaOH^+$ monolayer with diffusing HCO_3^- ions.

Statistical Analyses of Step Edge Structures and Dynamics. To obtain insights into the physical origins for the observed variations in the step edge structure, we investigated their dependence on the crystallographic orientation. Figure 6a

DOI: 10.1021/acs.jpcc.9b05788
J. Phys. Chem. C 2019, 123, 19786−19793

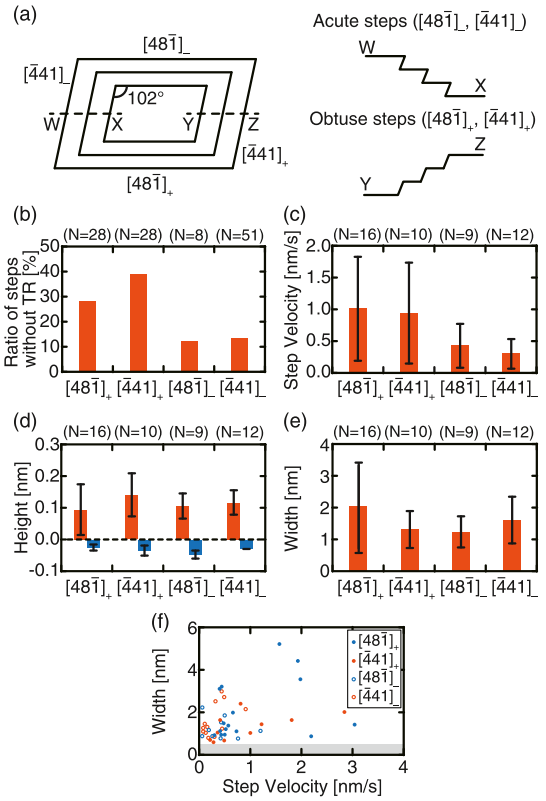

Figure 6. Statistical analysis of calcite step edge structures and dynamics observed by high-speed FM-AFM in water. (a) Schematic illustration of an etch pit formed on the dissolving calcite ($10\bar{1}4$) surface. (b) Ratio of the steps without a TR. (c–e) Dependence of (c) step velocity, and (d) height and (e) width of the TRs on the crystallographic orientation. (f) Dependence of the TR width on the step velocity. This data was obtained from the same dataset as those used for (c–e). Number of the steps (N) used for each statistical analysis is given in the figure.

shows the schematic illustration of the calcite steps with different orientations. The dissolution of a calcite surface progresses by the step retreats in the four different directions. These steps form a parallelogram etch pit with the angles between the two adjacent steps of 102° and 78°. The two opposing steps form a pair of acute ($[\bar{4}41]_-$ and $[48\bar{1}]_-$) or obtuse ($[\bar{4}41]_+$ and $[48\bar{1}]_+$) steps as shown in Figure 6a.

We performed FM-AFM imaging of various steps at random positions and statistically analyzed the obtained images. The result shows that the ratio of the steps without a TR is 29–39% for the obtuse steps and 13–14% for the acute steps (Figure 6b). These values suggest that the steps without a TR are less common for both crystallographic orientations, but they are more frequently observed for the obtuse steps.

For the steps with a TR, we have analyzed the dependence of the step velocity, and the height and width of the TRs on the crystallographic orientation as shown in Figure 6c–e. Figure 6c shows that the average velocity of the obtuse step (~1.0 nm/s) is faster than that of the acute steps (~0.5 nm/s). This is consistent with the results reported by the previous studies, where the faster velocity of the obtuse steps is attributed to the lower free-energy change caused by the sequential removals of the ions from the step edge.[43,44]

Figure 6d shows the average height of the TRs. In this experiment, 65% of the TRs were imaged as a protrusion (e.g., Figure 1b), while the rest were imaged as a depression (e.g., Figure 3a). The positive and negative heights shown in Figure 6d were obtained by independently averaging the heights of these two types of TRs. For both the positive and negative heights, no strong dependence on the orientations was observed. Similarly, the average width of the TRs shows no significant dependence on the orientation as shown in Figure 6e. We also confirmed that there is no significant dependence between the average width of the TR and the step velocity as shown in Figure 6f. These results reveal that the probability of the TR formation depends on the crystallographic orientation but, once it is formed, its properties do not depend on the crystallographic orientation or the step velocity.

Figure 6b,c suggests that a TR is more frequently formed along the slowly dissolving acute steps than along the rapidly dissolving obtuse steps. In addition, almost no step movement was observed during the TR formation (Figure 5). These results consistently suggest that the slow dissolution condition is favorable for the TR formation. Although we were able to observe the TR formation, the disappearance of a TR has not been observed. In addition, our statistical analysis suggests that the steps without a TR are less common. These results imply that the steps with a TR may be thermodynamically favorable than those without a TR. In the meanwhile, the coexistence of the step edges with and without a TR suggests that the energetic barrier to form a TR is comparable to that for the removal of ions directly from the step edges. Therefore, the subtle difference in the free energy to remove the ions from the acute and obtuse steps[44] can lead to the difference in the probability of the TR formation.

■ CONCLUSIONS

In this study, we have performed the systematic study on the TR observed by high-speed FM-AFM during the calcite dissolution in water. By statistically analyzing a large number of atomic-scale images of the calcite step edges, we obtained important findings on the mechanisms of both the FM-AFM imaging and calcite dissolution.

The FM-AFM images of the TRs show several variations, including a protrusion, depression, and two-divided steps with and without a depression. These variations can be explained by the different tip trajectories on the different hydration layers formed on the same step edge structure with a TR. Such variations in the tip trajectory are probably caused by the differences in the tip structures and/or the local ion concentration. These results demonstrate that the atomic-scale contrasts in the high-speed FM-AFM images are sensitive to the local hydration structures and ion concentration. This can make the image interpretation complicated yet may help us to visualize subtle differences that cannot be visualized by other techniques. In fact, the capability of FM-AFM to visualize the hydration structure allowed us to find the TRs and their variations for the first time. This capability should also be useful for investigating atomistic processes at the step edges of various crystals during their growth or dissolution.

The majority of the calcite steps in the dissolution condition has a TR (~77%). However, we also confirmed the existence of the steps without a TR. The ratio between them shows clear dependence on the crystallographic orientation: the acute steps more frequently show a TR than the obtuse steps. This result and direct imaging of the formation of the TR suggest that the free energy to form a TR is comparable to that for removing ions directly from the step edge, and an increase in the local ionic strength may alter this balance to facilitate the TR

DOI: 10.1021/acs.jpcc.9b05788
J. Phys. Chem. C 2019, 123, 19786–19793

formation. Once the TR is formed, its properties such as the width and height do not depend on the crystallographic orientation or the step velocity. These findings of the statistical properties of the TR will allow us to quantitatively correlate the atomistic step edge structures having a large variation with the averaged macroscopic properties reported by the previous studies. Such multiscale understanding of the calcite dissolution mechanism should lead to the future improvements in the prediction and simulation of the various phenomena related to the global carbon cycles, fabrication of optical components and biomineralizations.

■ ASSOCIATED CONTENT

Supporting Information

The Supporting Information is available free of charge on the ACS Publications website at DOI: 10.1021/acs.jpcc.9b05788.

Backward scan FM-AFM images of calcite surface in water; FM-AFM images of calcite surface in water obtained with different Δf; and discussions on possible influence of scan artifacts (PDF)

Successive FM-AFM images of calcite $(10\bar{1}4)$ surface obtained in water (MP4)

Successive FM-AFM images of calcite $(10\bar{1}4)$ surface obtained in water (MP4)

Successive FM-AFM images of calcite $(10\bar{1}4)$ surface obtained in water (MP4)

Successive FM-AFM images of calcite $(10\bar{1}4)$ surface obtained in water (MP4)

Successive FM-AFM images of calcite $(10\bar{1}4)$ surface obtained in water (MP4)

Successive FM-AFM images of calcite $(10\bar{1}4)$ surface obtained in water (MP4)

■ AUTHOR INFORMATION

Corresponding Authors

*E-mail: adam.foster@aalto.fi (A.S.F.).

*E-mail: fukuma@staff.kanazawa-u.ac.jp (T.F.).

ORCID

Adam S. Foster: 0000-0001-5371-5905

Takeshi Fukuma: 0000-0001-8971-6002

Notes

The authors declare no competing financial interest.

■ ACKNOWLEDGMENTS

This work was supported by World Premier International Research Center Initiative (WPI), MEXT, Japan; JSPS KAKENHI grant number 16H02111; JST Mirai-Project (no. 18077272); Advanced Technology Institute Research Grants 2017; and CHOZEN Project, Kanazawa University. Computing resources from the Aalto Science-IT project and CSC, Helsinki are gratefully acknowledged. A.S.F. was supported by the Academy of Finland (project no. 314862).

■ REFERENCES

(1) Reeder, R. J. In *Carbonates, Mineralogy, and Chemistry: Reviews in Mineralogy*; Reeder, R. J., Ed.; Mineralogical Society of America, 1983.

(2) Sigman, D. M.; Boyle, E. A. Glacial/Interglacial Variations in Atmospheric Carbon Dioxide. *Nature* **2000**, *407*, 859−869.

(3) Sarmiento, J.; Gruber, N. *Ocean Biogeochemical Dynamics*; Princeton University Press, 2006.

(4) Zeebe, R. E.; Zachos, J. C.; Caldeira, K.; Tyrrell, T. Carbon Emissions and Acidification. *Science* **2008**, *321*, 51−52.

(5) Teng, H. H.; Dove, P. M. Surface Site-Specific Interactions of Aspartate with Calcite During Dissolution; Implications for Biomineralization. *Am. Mineral.* **1997**, *82*, 878−887.

(6) Sand, K. K.; Pedersen, C. S.; Sjöberg, S.; Nielsen, J. W.; Makovicky, E.; Stipp, S. L. S. Biomineralization: Long-Term Effectiveness of Polysaccharides on the Growth and Dissolution of Calcite. *Cryst. Growth Des.* **2014**, *14*, 5486−5494.

(7) Moropoulou, A.; Bisbikou, K.; Torfs, K.; Van Grieken, R.; Zezza, F.; Macri, F. Origin and Growth of Weathering Crusts on Ancient Marbles in Industrial Atmosphere. *Atmos. Environ.* **1998**, *32*, 967−982.

(8) Knauss, K. G.; Johnson, J. W.; Steefel, C. I. Evaluation of the impact of CO_2, Co-Contaminant Gas, Aqueous Fluid and Reservoir Rock Interactions on the Geologic Sequestration of CO_2. *Chem. Geol.* **2005**, *217*, 339−350.

(9) Truesdale, V. W. Evidence and Potential Implications of Exponential Tails to Concentration Versus Time Plots for the Batch Dissolution of Calcite. *Aquat. Geochem.* **2015**, *21*, 365−396.

(10) Shiraki, R.; Rock, P. A.; Casey, W. H. Dissolution Kinetics of Calcite in 0.1 M NaCl Solution at Room Temperature: An Atomic Force Microscopic (AFM) Study. *Aquat. Geochem.* **2000**, *6*, 87−108.

(11) Hillner, P. E.; Gratz, A. J.; Manne, S.; Hansma, P. K. Atomic-Scale Imaging of Calcite Growth and Dissolution in Real Time. *Geology* **1992**, *20*, 359−362.

(12) Stipp, S. L. S.; Eggleston, C. M.; Nielsen, B. S. Calcite Surface Structure Observed at Microtopographic and Molecular Scales with Atomic Force Microscopy (AFM). *Geochim. Cosmochim. Acta* **1994**, *58*, 3023−3033.

(13) Arvidson, R. S.; Ertan, I. E.; Amonette, J. E.; Luttge, A. Variation in Calcite Dissolution Rates:A Fundamental Problem? *Geochim. Cosmochim. Acta* **2003**, *67*, 1623−1634.

(14) Lasaga, A. C.; Luttge, A. Variation of Crystal Dissolution Rate Based on a Dissolution Stepwave Model. *Science* **2001**, *291*, 2400−2404.

(15) Spagnoli, D.; Kerisit, S.; Parker, S. C. Atomistic Simulation of the Free Energies of Dissolution of Ions from Flat and Stepped Calcite Surfaces. *J. Cryst. Growth* **2006**, *294*, 103−110.

(16) De La Pierre, M.; Raiteri, P.; Gale, J. D. Structure and Dynamics of Water at Step Edges on the Calcite {10-14} Surface. *Cryst. Growth Des.* **2016**, *16*, 5907.

(17) McCoy, J. M.; LaFemina, J. P. Kinetic Monte Carlo Investigation of Pit Formation at the $CaCO_3$ (1014) Surface-Water Interface. *Surf. Sci.* **1997**, *373*, 288−299.

(18) Kurganskaya, I.; Luttge, A. Kinetic Monte Carlo Approach To Study Carbonate Dissolution. *J. Phys. Chem. C* **2016**, *120*, 6482−6492.

(19) Lardge, J. S.; Duffy, D. M.; Gillan, M. J.; Watkins, M. Ab Initio Simulations of the Interaction between Water and Defects on the Calcite (1014) Surface. *J. Phys. Chem. C* **2010**, *114*, 2664−2668.

(20) Kodera, N.; Yamamoto, D.; Ishikawa, R.; Ando, T. Video Imaging of Walking Myosin V by High-Speed Atomic Force Microscopy. *Nature* **2010**, *468*, 72−76.

(21) Fukuma, T.; Kobayashi, K.; Matsushige, K.; Yamada, H. True Atomic Resolution in Liquid by Frequency-Modulation Atomic Force Microscopy. *Appl. Phys. Lett.* **2005**, *87*, 034101.

(22) Fukuma, T.; Ueda, Y.; Yoshioka, S.; Asakawa, H. Atomic-Scale Distribution of Water Molecules at the Mica-Water Interface Visualized by Three-Dimensional Scanning Force Microscopy. *Phys. Rev. Lett.* **2010**, *104*, 016101.

(23) Fukuma, T.; Kimura, M.; Kobayashi, K.; Matsushige, K.; Yamada, H. Development of Low Noise Cantilever Deflection Sensor for Multienvironment Frequency-Modulation Atomic Force Microscopy. *Rev. Sci. Instrum.* **2005**, *76*, 053704.

(24) Fukuma, T.; Jarvis, S. P. Development of Liquid-Environment Frequency Modulation Atomic Force Microscope with Low Noise Deflection Sensor for Cantilevers of Various Dimensions. *Rev. Sci. Instrum.* **2006**, *77*, 043701.

DOI: 10.1021/acs.jpcc.9b05788
J. Phys. Chem. C 2019, 123, 19786−19793

(25) Fukuma, T. Wideband Low-Noise Optical Beam Deflection Sensor with Photothermal Excitation for Liquid-Environment Atomic Force Microscopy. *Rev. Sci. Instrum.* **2009**, *80*, 023707.
(26) Fukuma, T.; Onishi, K.; Kobayashi, N.; Matsuki, A.; Asakawa, H. Atomic-Resolution Imaging in Liquid by Frequency Modulation Atomic Force Microscopy Using Small Cantilevers with Megahertz-Order Resonance Frequencies. *Nanotechnology* **2012**, *23*, 135706.
(27) Miyata, K.; Usho, S.; Yamada, S.; Furuya, S.; Yoshida, K.; Asakawa, H.; Fukuma, T. Separate-Type Scanner and Wideband High-Voltage Amplifier for Atomic-Resolution and High-Speed Atomic Force Microscopy. *Rev. Sci. Instrum.* **2013**, *84*, 043705.
(28) Akrami, S. M. R.; Miyata, K.; Asakawa, H.; Fukuma, T. Note: High-Speed Z Tip Scanner with Screw Cantilever Holding Mechanism for Atomic-Resolution Atomic Force Microscopy in Liquid. *Rev. Sci. Instrum.* **2014**, *85*, 126106.
(29) Mitani, Y.; Kubo, M.; Muramoto, K.-i.; Fukuma, T. Wideband Digital Frequency Detector with Subtraction-Based Phase Comparator for Frequency Modulation Atomic Force Microscopy. *Rev. Sci. Instrum.* **2009**, *80*, 083705.
(30) Miyata, K.; Asakawa, H.; Fukuma, T. Real-Time Atomic-Resolution Imaging of Crystal Growth Process in Water by Phase Modulation Atomic Force Microscopy at One Frame per Second. *Appl. Phys. Lett.* **2013**, *103*, 203104.
(31) Miyata, K.; Fukuma, T. Quantitative Comparison of Wideband Low-Latency Phase-Locked Loop Circuit Designs for High-Speed Frequency Modulation Atomic Force Microscopy. *Beilstein J. Nanotechnol.* **2018**, *9*, 1844−1855.
(32) Miyata, K.; Tracey, J.; Miyazawa, K.; Haapasilta, V.; Spijker, P.; Kawagoe, Y.; Foster, A. S.; Tsukamoto, K.; Fukuma, T. Dissolution Processes at Step Edges of Calcite in Water Investigated by High-Speed Frequency Modulation Atomic Force Microscopy and Simulation. *Nano Lett.* **2017**, *17*, 4083−4089.
(33) Orme, C. A.; Noy, A.; Wierzbicki, A.; McBride, M. T.; Grantham, M.; Teng, H. H.; Dove, P. M.; DeYoreo, J. J. Formation of Chiral Morphologies Through Selective Binding of Amino Acids to Calcite Surface Steps. *Nature* **2001**, *411*, 775−779.
(34) Nada, H. Difference in the Conformation and Dynamics of Aspartic Acid on the Flat Regions, Step Edges, and Kinks of a Calcite Surface: A Molecular Dynamics Study. *J. Phys. Chem. C* **2014**, *118*, 14335.
(35) Tracey, J.; Miyazawa, K.; Spijker, P.; Miyata, K.; Reischl, B.; Canova, F. F.; Rohl, A. L.; Fukuma, T.; Foster, A. S. Understanding 2D Atomic Resolution Imaging of the Calcite Surface in Water by Frequency Modulation Atomic Force Microscopy. *Nanotechnology* **2016**, *27*, 415709.
(36) Fukuma, T.; Higgins, M. J.; Jarvis, S. P. Direct Imaging of Individual Intrinsic Hydration Layers on Lipid Bilayers at Ångstrom Resolution. *Biophys. J.* **2007**, *92*, 3603−3609.
(37) Akrami, S. M. R.; Nakayachi, H.; Watanabe-Nakayama, T.; Asakawa, H.; Fukuma, T. Significant Improvements in Stability and Reproducibility of Atomic-Scale Atomic Force Microscopy in Liquid. *Nanotechnology* **2014**, *25*, 455701.
(38) Fukuma, T.; Reischl, B.; Kobayashi, N.; Spijker, P.; Canova, F. F.; Miyazawa, K.; Foster, A. S. Mechanism of Atomic Force Microscopy Imaging of Three-Dimensional Hydration Structures at a Solid-Liquid Interface. *Phys. Rev. B: Condens. Matter Mater. Phys.* **2015**, *92*, 155412.
(39) Reischl, B.; Watkins, M.; Foster, A. S. Free Energy Approaches for Modeling Atomic Force Microscopy in Liquids. *J. Chem. Theory Comput.* **2013**, *9*, 600−608.
(40) Plimpton, S. Fast Parallel Algorithms for Short-Range Molecular Dynamics. *J. Comp. Physiol.* **1995**, *117*, 1−19.
(41) Humphrey, W.; Dalke, A.; Schulten, K. VMD: Visual Molecular Dynamics. *J. Mol. Graph. Model.* **1996**, *14*, 33−38.
(42) Michaud-Agrawal, N.; Denning, E. J.; Woolf, T. B.; Beckstein, O. MDAnalysis: A Toolkit for the Analysis of Molecular Dynamics Simulations. *J. Comput. Chem.* **2011**, *32*, 2319−2327.
(43) De Giudici, G. Surface Control Vs. Diffusion Control During Calcite Dissolution: Dependence of Step-Edge Velocity upon Solution pH. *Am. Mineral.* **2002**, *87*, 1279−1285.
(44) Kerisit, S.; Parker, S. C.; Harding, J. H. Atomistic Simulation of the Dissociative Adsorption of Water on Calcite Surfaces. *J. Phys. Chem. B* **2003**, *107*, 7676−7682.

DOI: 10.1021/acs.jpcc.9b05788
J. Phys. Chem. C 2019, 123, 19786−19793